

Uncertainty relations and minimum uncertainty states for the discrete Fourier transform and the Fourier series

G W Forbes¹, M A Alonso² and A E Siegman³

¹ QED Technologies Inc, 1040 University Ave, Rochester, NY 14607, USA

² Centro de Ciencias Físicas, Universidad Nacional Autónoma de México, Apdo. Postal 48-3, Cuernavaca Mor. 62260, Mexico

³ Edward L. Ginzton Laboratory and Department of Electrical Engineering, Stanford University, Stanford, CA 94305, USA

E-mail: forbes@qedmrf.com, alonso@fis.unam.mx and siegman@stanford.edu

Received 24 February 2003, in final form 24 April 2003

Published DD MMM 2003

Online at stacks.iop.org/JPhysA/36/1

Abstract

The conventional Fourier transform has a well-known uncertainty relation that is defined in terms of the first and second moments of both a function and its Fourier transform. It is also well known that Gaussian functions, when translated to an arbitrary centre and supplemented by a linear phase factor, provide a complete set of minimum uncertainty states (MUSs) that exactly satisfies this uncertainty relation. A similarly general set of MUSs and uncertainty relations are derived here for discrete and/or periodic generalizations of the Fourier transform, namely for the discrete Fourier transform and the Fourier series. These extensions require a modified definition for the width of a periodic distribution, and they lead to more complex uncertainty relations that turn out to depend on the centroid location and mean frequency of the distribution. The derivations lead to novel generalizations of Hermite–Gaussian functions and, like Gaussians, the MUSs can play a special role in a range of Fourier applications.

PACS number:

See endnote 1

1. Introduction

The uncertainty relation for the Fourier transformation (FT) specifies a minimum value for the product of the spread of a function and that of its Fourier conjugate. It was recently shown [1] that this relation can be derived from an analogous result for the discrete Fourier

transformation (DFT). A similar inequality was also derived in [1] for the Fourier series (FS). That is, by considering appropriate limits, uncertainty relations for both the FT and the FS have been shown to follow from a corresponding inequality for the DFT. Since the FS and DFT cases involve periodic distributions, a modified measure of spread must be introduced to replace the usual second-moment-based measure. Two observations reveal that the DFT result serves as a unique foundation for these inequalities. First, in the limit of high localization, the non-standard measure of spread *irreversibly* reduces to the usual variance. Second, a function and its Fourier conjugate are *both* periodic only for the DFT. Several uncertainty measures and associated relations for the FS and the DFT have been proposed within the area of quantum optics, where a relation is sought between the spreads in the phase and the number of photons. For a summary of this body of work, see the review article by Pegg and Barnett [2].

Although the lower bound set by the uncertainty relation for the FT is attained by well-known minimum uncertainty states (namely Gaussian functions), this is not so for the DFT. That is, the inequality for the discrete case is weaker than it could be. A stronger (but more complicated) inequality can be found by explicitly constructing the associated minimum uncertainty states (MUSs). This approach turns out to be akin to de Bruijn's derivation [3] of the familiar uncertainty relation. It involves the decomposition of any given distribution in terms of a basis of Hermite–Gaussian functions. The lowest order member is precisely a Gaussian, and de Bruijn's method shows this to be a MUS.

In fact, Opatrný [4] has derived some preliminary results on stronger uncertainty relations for the DFT. The generalization of the process of Hermite–Gaussian decomposition was not considered in that work, however. Further, his analogues of Gaussians for discrete periodic functions are limited to periodic sequences, say $\{a_m | m = 0, 1, 2, \dots, M - 1\}$ with $a_{m+M} = a_m$, that are symmetric about a sample point. So, for example, $a_m = a_{-m}$ when the centre of symmetry is chosen to fall at $m = 0$. However, it is also natural to consider whether there is a periodic and discrete analogue of a Gaussian distribution that is symmetric about a mid-point, i.e. $a_m = a_{1-m}$. More generally, could there be MUSs that resemble samples from a Gaussian curve that is centred at an arbitrary position with respect to the sample points?

In its most general form, Hermite–Gaussian decomposition involves freedom in choosing not only the centre of the associated Gaussian factor, but also its width and the frequency of the linear phase factor that can be placed across the entire basis (i.e. the centre in Fourier space). These freedoms are often essential to achieving an effective decomposition (i.e. smallest rms residual for a fixed number of coefficients). If such freedoms were found for a discrete analogue of the Hermite–Gaussian functions, they would open new options for a fractional DFT because the possibility of varying the centre of the underlying Gaussian has not been considered in this application [5–7]. We show that this is possible and that the same approach is also applicable for the FS.

A central goal in the current work, therefore, is the definition of periodic generalizations of the Hermite–Gaussian functions. These definitions are required to include the ability to control the centre and width of the zeroth member as well as its mean frequency. By starting with the discrete case and taking appropriate limits (as in [1]), it turns out that it is possible to extract either a set of continuous periodic analogues of the Hermite–Gaussians or the conventional non-periodic forms. The derivation presented here also establishes that some of the members of these basis sets are indeed MUSs. There are some unexpected surprises, however. To smooth the way, the general method is introduced in section 2 by rederiving familiar results for the FT. These results are subsequently extended to the DFT in section 3, and briefly sketched out for the FS in section 4.

2. MUSs for the Fourier transformation

The FT and its inverse are taken to be given by

$$F(p) := \frac{1}{\sqrt{2\pi}} \int f(x) e^{-ipx} dx \quad (2.1a)$$

$$f(x) = \frac{1}{\sqrt{2\pi}} \int F(p) e^{ipx} dp \quad (2.1b)$$

where ‘:=’ denotes a definition. It follows immediately that

$$\begin{aligned} \int f(x)g^*(x) dx &= \int \left[\frac{1}{\sqrt{2\pi}} \int F(p) e^{ipx} dp \right] g^*(x) dx \\ &= \int F(p) \left[\frac{1}{\sqrt{2\pi}} \int g(x) e^{-ipx} dx \right]^* dp \\ &= \int F(p)G^*(p) dp. \end{aligned} \quad (2.2)$$

By choosing $g = f$, the norm of f is found to satisfy $\|f\|^2 := \int |f(x)|^2 dx = \int |F(p)|^2 dp$.

The familiar uncertainty relation is expressed in terms of moments,

$$\overline{x^j} := \frac{1}{\|f\|^2} \int x^j |f(x)|^2 dx \quad (2.3a)$$

$$\overline{p^j} := \frac{1}{\|f\|^2} \int p^j |F(p)|^2 dp = \frac{1}{\|f\|^2} \int f^*(x) \left(-i \frac{d}{dx} \right)^j f(x) dx \quad (2.3b)$$

where equation (2.2) is used in equation (2.3b). In these terms, the usual measures of spread for f and F are given by

$$\Delta_f := [(\overline{(x - \bar{x})^2})]^{1/2} = (\overline{x^2} - \bar{x}^2)^{1/2} \quad (2.4a)$$

$$\Delta_F := (\overline{p^2} - \bar{p}^2)^{1/2}. \quad (2.4b)$$

Since the Fourier transform of $f(x - y) e^{iqx}$ is seen from equation (2.1a) to be $F(p - q) e^{-i(p-q)y}$, it is possible to force $\bar{x} = \bar{p} = 0$ without changing either Δ_f or Δ_F : just use $y = \bar{x}$ and $q = \bar{p}$. It is sufficient therefore to derive uncertainty relations, and to seek MUSs, with the assumption that $\bar{x} = \bar{p} = 0$. In this case, $\Delta_f^2 = \overline{x^2}$ and $\Delta_F^2 = \overline{p^2}$. However, things are not so straightforward for the DFT, so we take a more general approach here to pave the way. Although it may appear to be a roundabout path at first sight, this analysis is vital for clarifying the twists and turns of the DFT case.

2.1. Basics of a variational construction

Although de Bruijn’s derivation proceeds by using recurrence relations for the Hermite–Gaussians, it is more helpful in our analysis to derive a differential equation that defines these functions. This equation follows from the fact that we wish to minimize one functional (say the spread in frequency space) while satisfying a set of functional constraints (e.g., a fixed spread in coordinate space and prescribed first moments in both spaces). As a result, a linear combination of the functional derivatives must vanish identically. The associated linear coefficients are called the Lagrange multipliers. Note that the functionals and the Lagrange multipliers are all real valued, and the latter must be chosen to enforce the desired values for the constraints.

The functionals of interest here depend on the real and imaginary parts of f , say $f(x) = u(x) + iv(x)$, and perhaps on their derivatives. For a functional of the form

$$\phi = \int G[x, u(x), u'(x)] dx \quad (2.5)$$

the functional derivative is written here as $\delta\phi/\delta u$ and is defined so that the change in ϕ that results from replacing $u(x)$ by $u(x) + \varepsilon(x)$ is given to first order by

$$\Delta\phi = \int \frac{\delta\phi}{\delta u}[x, u(x), u'(x)]\varepsilon(x) dx. \quad (2.6)$$

After replacing both $u(x)$ and $u'(x)$ in equation (2.5), Taylor expanding and then integrating one of the terms by parts, $\delta\phi/\delta u$ is found to be given by

$$\frac{\delta\phi}{\delta u}[x, u(x), u'(x)] = \frac{\partial G}{\partial u}[x, u(x), u'(x)] - \frac{d}{dx} \left\{ \frac{\partial G}{\partial u'}[x, u(x), u'(x)] \right\}. \quad (2.7)$$

The functionals of interest in this section involve u , u' , v and v' :

$$\phi_0 = \|f\|^2 = \int [u^2(x) + v^2(x)] dx \quad (2.8a)$$

$$\phi_1 = \|f\|^2 \bar{x} = \int x[u^2(x) + v^2(x)] dx \quad (2.8b)$$

$$\phi_2 = \|f\|^2 \bar{x}^2 = \int x^2[u^2(x) + v^2(x)] dx \quad (2.8c)$$

$$\phi_3 = \|f\|^2 \bar{p} = \int [v'(x) - iu'(x)][u(x) - iv(x)] dx \quad (2.8d)$$

$$\phi_4 = \|f\|^2 \bar{p}^2 = \int |f'(x)|^2 dx = \int [u'^2(x) + v'^2(x)] dx. \quad (2.8e)$$

All the constraints as well as the functional to be minimized can be written as simple algebraic combinations of these five basic entities. It follows that a linear combination of the functional derivatives must vanish identically. Equation (2.7) can be used to see that this condition can be expressed as

$$\begin{aligned} (0, 0) &\equiv \sum_k L_k \left(\frac{\delta\phi_k}{\delta u}, \frac{\delta\phi_k}{\delta v} \right) \\ &= 2[L_0(u, v) + L_1x(u, v) + L_2x^2(u, v) + L_3(v', -u') + L_4(u'', v'')] \end{aligned} \quad (2.9)$$

where L_k are the Lagrange multipliers. All entities in equation (2.9) are real, and if the first component of this identity is added to i times the second, it follows that any MUS must satisfy

$$L_4 f''(x) - iL_3 f'(x) + [L_0 + L_1x + L_2x^2]f(x) = 0. \quad (2.10)$$

Strictly speaking, there is one more Lagrange multiplier than necessary here: equations (2.9) and (2.10) can be divided through by, say, L_4 (which was included only as a formal convenience).

2.2. Hermite–Gaussian eigenstates

The next step is to find values for the Lagrange multipliers for which equation (2.10) possesses normalizable solutions. In particular, we will seek those with the desired values of \bar{x} , \bar{p} and Δ_f . By globally changing sign on all the Lagrange multipliers (which leaves equation (2.10) effectively unchanged), attention can be restricted to the case $L_2 > 0$ without loss of generality. It then turns out that, to admit normalizable solutions, L_4 must be negative. It is then convenient to multiply equation (2.10) throughout by $1/\sqrt{L_2|L_4|}$ so that it can be rewritten as

$$\hat{\Gamma} f(x) = \lambda f(x) \quad (2.11)$$

where

$$\hat{\Gamma}(w, s, t) := w^{-2}(x-s)^2 + w^2 \left(-i \frac{d}{dx} - t \right)^2. \quad (2.12)$$

(For compactness, the arguments of the operator $\hat{\Gamma}$ are typically omitted.) Upon expanding the right-hand side of equation (2.12) it is straightforward to compare equations (2.11) and (2.10) to find the unique map between the four independent values from among $\ell_k := L_k/\sqrt{L_2|L_4|}$ (hence $\ell_2 = -1/\ell_4$) and the new parameters, namely w , s , t and λ .

Equation (2.11) has solutions that remain finite in the limits of large x only for discrete values of λ , say $\lambda = \lambda_j$ where $j = 0, 1, 2, \dots$. These eigenfunctions of $\hat{\Gamma}$ satisfy

$$\hat{\Gamma} \psi^{(j)}(w, s, t; x) = \lambda_j \psi^{(j)}(w, s, t; x) \quad (2.13)$$

where λ_j may be expected to depend on w , s and t . It turns out that

$$\psi^{(j)}(w, s, t; x) = w^{-1/2} e^{ixt} h_j \left(\frac{x-s}{w} \right) \quad (2.14)$$

with

$$h_j(u) := H_j(u) e^{-u^2/2} / \sqrt{N_j}. \quad (2.15)$$

Here, $H_j(u)$ is the Hermite polynomial of order j , and the normalization constant is given by $N_j := \int H_j^2(u) e^{-u^2} du = 2^j j! \sqrt{\pi}$. The dimensionless eigenvalues turn out to be given by $\lambda_j = 2j + 1$. Since $\hat{\Gamma}$ is Hermitian, its eigensolutions are orthogonal and complete. That is, any function can be expressed in the form

$$f(x) = \sum_{j=0}^{\infty} c_j(w, s, t) \psi^{(j)}(w, s, t; x) \quad (2.16)$$

where

$$c_j(w, s, t) := \int \psi^{(j)*}(w, s, t; x) f(x) dx. \quad (2.17)$$

2.3. Hermite–Gaussians as MUSs

Upon writing $(x-s) = [(x-\bar{x}) - (s-\bar{x})]$ and doing the same for the conjugate term, it is easy to show from equation (2.12) that

$$\int f^*(x) \hat{\Gamma} f(x) dx = \{w^{-2} [\Delta_f^2 + (\bar{x}-s)^2] + w^2 [\Delta_F^2 + (\bar{p}-t)^2]\} \|f\|^2. \quad (2.18)$$

Alternatively, it follows from equations (2.13), (2.16), (2.17) and the linearity of $\hat{\Gamma}$ that

$$\begin{aligned}
\int f^*(x) \hat{\Gamma} f(x) dx &= \int f^*(x) \hat{\Gamma} \sum_{j=0}^{\infty} c_j(w, s, t) \psi^{(j)}(w, s, t; x) dx \\
&= \int f^*(x) \sum_{j=0}^{\infty} c_j(w, s, t) \lambda_j \psi^{(j)}(w, s, t; x) dx \\
&= \sum_{j=0}^{\infty} \lambda_j c_j(w, s, t) \left[\int \psi^{(j)}(w, s, t; x) f^*(x) dx \right] \\
&= \sum_{j=0}^{\infty} \lambda_j |c_j(w, s, t)|^2.
\end{aligned} \tag{2.19}$$

It follows similarly that

$$\|f\|^2 := \int |f(x)|^2 dx = \sum_{j=0}^{\infty} |c_j(w, s, t)|^2. \tag{2.20}$$

Equations (2.18), (2.19) and (2.20) lead immediately to

$$w^{-2} [\Delta_f^2 + (\bar{x} - s)^2] + w^2 [\Delta_F^2 + (\bar{p} - t)^2] = \frac{\sum_{j=0}^{\infty} \lambda_j |c_j(w, \bar{x}, \bar{p})|^2}{\sum_{j=0}^{\infty} |c_j(w, \bar{x}, \bar{p})|^2} \geq \lambda_0 = 1. \tag{2.21}$$

The inequality in equation (2.21) follows upon reducing the numerator by replacing λ_j by λ_0 throughout the sum.

When values are prescribed for Δ_f , \bar{x} and \bar{p} , it is straightforward to solve equation (2.21) to find a lower bound for Δ_F . The resulting relation is necessarily satisfied for all values of w , s and t . These values can thus be chosen to maximize this lower bound. This leads to $s = \bar{x}$, $t = \bar{p}$ and $w^{-2} = 1/(2\Delta_f^2)$, and the standard Fourier uncertainty relation results:

$$\Delta_f \Delta_F \geq \frac{1}{2}. \tag{2.22}$$

An alternative approach leads directly to the MUSs, however. It follows from equation (2.21) that the inequality becomes an equality when $f(x)$ is precisely the ground state, i.e. only the first term in each of the sums is non-zero. The goal instead, therefore, is to choose values for w , s and t to ensure that the properties of the resulting ground state match the desired values of Δ_f , \bar{x} and \bar{p} . Since the ground state is given explicitly by equation (2.14), this process is straightforward. It again turns out that $s = \bar{x}$, $t = \bar{p}$ and $w^{-2} = 1/(2\Delta_f^2)$, but now for a different reason. As a result, the only MUSs (i.e. states that attain the limit set by equation (2.22)) are proportional to

$$\psi^{(0)}(w, \bar{x}, \bar{p}; x) = w^{-1/2} \pi^{-1/4} e^{i\bar{p}x} e^{-(x-\bar{x})^2/2w^2} \tag{2.23}$$

for any positive w and real values of \bar{x} and \bar{p} . This result sets the expectation that MUSs should be sought for the DFT with any prescribed values for the width, centroid location, and mean frequency. The generalization of this treatment to the case of discrete periodic functions is the principal goal of what follows.

3. MUSs for the discrete Fourier transformation

The DFT and its inverse map the periodic sequence $\{a_m : m = 0, 1, 2, \dots, M - 1\}$ to its conjugate sequence and back via

$$A_n := \frac{1}{\sqrt{M}} \sum_m a_m e^{-i2\pi mn/M} \quad (3.1a)$$

$$a_n = \frac{1}{\sqrt{M}} \sum_m A_m e^{i2\pi mn/M}. \quad (3.1b)$$

The periodicity of these sequences, i.e. $a_{m+M} = a_m$ and $A_{m+M} = A_m$ for all m , follows directly from these relations. Unless indicated otherwise, all sums are taken over a full period. A couple of standard properties of the DFT are used repeatedly below. First, shifting a sequence generates a phase on the conjugate sequence:

$$\begin{aligned} \frac{1}{\sqrt{M}} \sum_m a_{m+j} e^{-i\frac{2\pi}{M}mn} &= \frac{1}{\sqrt{M}} \sum_{m'} a_{m'} e^{-i\frac{2\pi}{M}(m'-j)n} \\ &= e^{i2\pi jn/M} A_n. \end{aligned} \quad (3.2)$$

Also, an analogue of equation (2.2) follows in the familiar manner:

$$\sum_m a_m^* b_m = \sum_m A_m^* B_m. \quad (3.3)$$

Note that there is a clear distinction between coordinate space and frequency space in the previous section, and this has traditionally allowed for careless notation. For example, if we are considering the distribution $f(x)$, it is dimensionally inconsistent to write $f(p)$ as a rule, thus \bar{x} necessarily characterizes f and not F . However, since it is meaningful to write both a_m and A_m , it is now awkward to distinguish properties of a sequence by using notation such as \bar{m} or Δ_m ; it is better to involve the kernel symbol itself in place of the index (i.e. use a or A instead of m). It turns out that the notions of centroids and spreads of periodic distributions also raise more significant difficulties [8]. Some of these issues are now reviewed before we consider minimum uncertainty. Appropriate notation is introduced as part of this discussion.

3.1. Uncertainty relation for the DFT

Moments of m do not respect the periodicity of a_m : instead of being at the far end of the sequence, a_{M-1} is effectively an immediate neighbour of a_0 . That is, the sequence effectively resides on a ring. Definitions of centroid and width that respect this property were applied by Bandilla and Paul [1, 4, 9]. The relevant ideas follow naturally upon considering the centre of mass of an array of weights that are uniformly distributed around the rim of the unit disc and have masses proportional to $|a_m|^2$, and similarly for the conjugate domain,

$$S_a := \frac{1}{\|a\|^2} \sum_m |a_m|^2 \exp\left(i\frac{2\pi}{M}m\right) = \frac{1}{\|a\|^2} \sum_m A_m^* A_{m-1} \quad (3.4a)$$

$$S_A := \frac{1}{\|a\|^2} \sum_m |A_m|^2 \exp\left(i\frac{2\pi}{M}m\right) = \frac{1}{\|a\|^2} \sum_m a_m^* a_{m+1} \quad (3.4b)$$

where $\|a\|$ is the norm of the sequences:

$$\|a\|^2 := \sum_m |a_m|^2 = \sum_m |A_m|^2. \quad (3.5)$$

(The second equality in each of equations (3.4a), (3.4b) and (3.5) follows directly from equations (3.2) and (3.3).) The centroid and width of a_m can now be characterized by

$$\mu_a := \frac{M}{2\pi} \arg(S_a) \quad (3.6a)$$

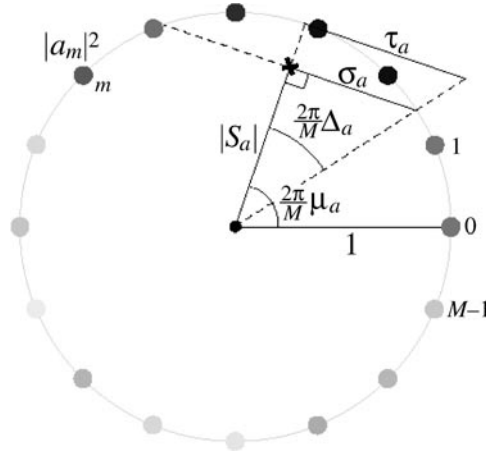


Figure 1. Once a periodic sequence is mapped to point masses that are uniformly distributed around the perimeter of a unit disc, measures of the spread and centroid of the sequence follow intuitively as shown. The centre of mass is marked as a cross. Either σ_a , τ_a , or Δ_a , can be used as measures of spread, while μ_a characterizes the sequence's centroid location.

$$\tau_a := \sqrt{1 - |S_a|^2} / |S_a| \quad (3.6b)$$

where \arg is taken to return a value between 0 and 2π . Those for the conjugate sequence are found by replacing a throughout equations (3.6a) and (3.6b) by A .

Note that, in contrast to the moments of m , a shift in the interval of summation in equations (3.4)–(3.5) does not change the results; all that is required is that the sums extend over a full period. As illustrated in figure 1, μ_a is the index value (modulo M) for the distribution's centroid. On the other hand, τ_a may be appreciated better by observing that it changes from zero to infinity as the centre of mass, i.e. S_a , moves from the edge of the unit disc in towards the centre. This is in keeping with the associated level of localization in the distributions that can lead to these positions for the centre of mass. More specifically, notice that $\sqrt{1 - |S_a|^2}$ is just half of the length of the shortest chord that contains the centre of mass. Therefore τ_a is just the tangent of the angle subtended at the disc's centre by half of this chord. For some applications, it may be more intuitive to convert this angle to a corresponding change in index by using much the same process as in equation (3.6a), i.e. consider $\Delta_a := (M/2\pi) \tan^{-1}(\tau_a)$. There are a number of such options, but the essential idea is that the localization increases with $|S_a|$. Also note that, when $|S_a|$ is zero, there is no preferred direction in the distribution and it is satisfying therefore that $\arg(S_a)$, hence μ_a , is no longer well defined.

In these terms, it was shown in [1] that the uncertainties for a DFT pair must satisfy a relation that resembles equation (2.22):

$$\tau_a \tau_A \geq \sin(\pi/M). \quad (3.7)$$

As indicated in the introduction, because there are no sequences that attain the associated lower bound on τ_A for a given (finite and non-zero) value of τ_a , this inequality can be strengthened by directly constructing MUSs. Following the comments at the end of section 2 regarding complete sets of MUSs, we now anticipate specifying a MUS by prescribing values for its width, its mean index value and its mean frequency. As a result, it is plausible that the lower limit on τ_A may now depend not only on τ_a , but also on μ_a and μ_A . We show in what follows that this is indeed the case.

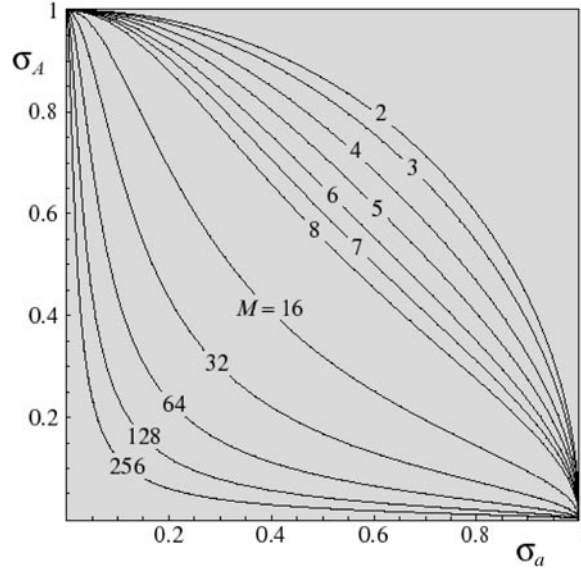


Figure 2. For any M , the algebraic relation in equation (3.8) indicates that the spreads for all sequences and their DFT conjugates must map to points that sit above a particular curve within the unit square having coordinates (σ_a, σ_A) . The curves are shown here for selected values of M . For $M \neq 2$, however, it turns out that these boundaries can be tightened because no states approach any point on the curves other than their common endpoints.

For graphical purposes, it is convenient to express equation (3.7) in terms of a measure of spread that is bounded. For example, we can use the sine of the angle mentioned in the previous paragraph, i.e. $\sigma_a := \sqrt{1 - |S_a|^2}$, which varies from zero (when the distribution is localized at a single point) to unity (when it is maximally delocalized). In these terms, equation (3.7) becomes

$$(\sigma_a^2 + T^2)(\sigma_A^2 + T^2) \geq T^2(1 + T^2) \quad (3.8)$$

where $T := \tan(\pi/M)$. As shown in figure 2, in the space with coordinates (σ_a, σ_A) , only the unit square is accessible, and equation (3.8) excludes a region of this square. The excluded region shrinks as M grows. Extending these excluded regions to their maximal size is one of the main goals of what follows. More generally, we consider the lower limit on σ_A as a function of σ_a , μ_a and μ_A (as well as M , of course). This is obviously more difficult to present graphically. Note, however, that the lower limit can depend only on the fractional parts of μ_a and μ_A . This is a consequence of the option of shifting a sequence by an integral number of sample spaces and of also generating an integral shift in its conjugate sequence by including a periodic linear phase (see equation (3.2)). Further, by swapping a_m and a_{-m} (which changes the sign of μ_a but leaves σ_a unchanged), it is clear that we need consider values of μ_a only between 0 and $\frac{1}{2}$. Similarly, since a_m can be replaced by a_m^* (which swaps A_m and A_{-m}), we can also restrict attention to μ_A between 0 and $\frac{1}{2}$.

The domain to be explored is evidently further reduced by the fact that the centre of mass necessarily falls within the polygon that connects the point masses on the ring of figure 1. That is, $|S_a|$ and $\arg(S_a)$ —hence σ_a and μ_a —cannot be prescribed arbitrarily. For $M = 1$, the centroid is always at the edge of the ring for both the original sequence and its conjugate, so $\sigma_a = \sigma_A = 0$ and $\mu_a = \mu_A = 0$. Since equation (3.8) reduces to $\sigma_a^2 \sigma_A^2 \geq 0$, all non-zero sequences are therefore MUSs for this trivial case. For $M = 2$, the polygon is just a line

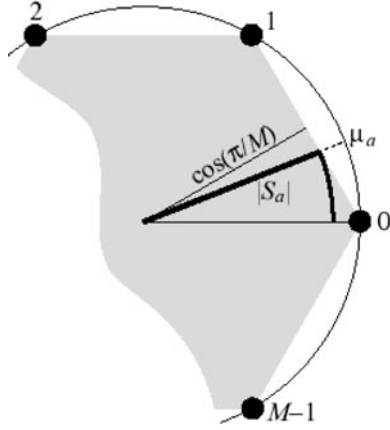


Figure 3. The centre of mass for a ring of M point masses must lie within the associated polygon. This brings intuitive constraints on μ_a and $|S_a|$.

segment, it is thus sufficient to consider only $\mu_a = \mu_A = 0$. As a result, the strengthened uncertainty relation will be able to be shown as a single curve. Note also that, in this case, equation (3.8) becomes $\sigma_a^2 + \sigma_A^2 \geq 1$. In fact, it is straightforward to show that any sequence of two real numbers satisfying $a_0 > a_1 > 0$ attains this limit. Translation and/or phasing (which amounts to interchanging the two elements and/or making a sign change on one element) then generate the complete set of MUSs for this simple case. In other words, equation (3.8) cannot be strengthened for $M \leq 2$.

For $M > 2$, it is evident that when the centroid is further from the origin than some points on the polygon, μ_a is then confined to a tighter domain. As indicated in figure 3, a simple geometric analysis of the polygon reveals that, when $|S_a| = \sqrt{1 - \sigma_a^2} \geq \cos(\pi/M)$, μ_a is now restricted by

$$0 \leq \mu_a \leq \frac{1}{2} - \frac{M}{2\pi} \cos^{-1} \left[\cos \left(\frac{\pi}{M} \right) / \sqrt{1 - \sigma_a^2} \right]. \quad (3.9)$$

In these cases, we can consider making multiple plots of the lower limit on σ_A as a function of σ_a for various fixed values of μ_a and μ_A between 0 and $\frac{1}{2}$. As a result of equation (3.9), these curves are defined only where

$$\sigma_a \geq \sqrt{\sin \left(\frac{2\pi}{M} \mu_a \right) \sin \left[\frac{2\pi}{M} (1 - \mu_a) \right]} / \cos \left[\frac{\pi}{M} (1 - 2\mu_a) \right]. \quad (3.10)$$

A similar relation holds with all subscripted a replaced by A . Together, these inequalities mean that strips of the unit square along the left and bottom edge in figure 2 are excluded by elementary considerations. The width of the excluded strips grows monotonically from zero at $\mu = 0$ to $\sin(\pi/M)$ at $\mu = \frac{1}{2}$. (Note that, in keeping with the comments of the previous paragraph, these strips exclude the entire domain unless $\mu_a = \mu_A = 0$ for $M = 2$.) For $M > 2$ and $\mu_a \neq 0$ and/or $\mu_A \neq 0$, the curves for the MUSs will now exclude part of this *truncated* unit square. The challenges are to determine just how much the relation in equation (3.8) can be strengthened for various values of M and $\mu_a, \mu_A \in [0, \frac{1}{2}]$, and what form the associated MUSs take.

3.2. Discrete analogues of Hermite–Gaussian functions

If a_m is separated into real and imaginary parts as $a_m = x_m + iy_m$, the analogues of the five functions in equations (2.8) take the form

$$\phi_0 = \|a\|^2 = \sum_n (x_n^2 + y_n^2) \quad (3.11a)$$

$$\phi_1 = \|a\|^2 \operatorname{Re}(S_a) = \sum_n (x_n^2 + y_n^2) \cos\left(\frac{2\pi}{M}n\right) \quad (3.11b)$$

$$\phi_2 = \|a\|^2 \operatorname{Im}(S_a) = \sum_n (x_n^2 + y_n^2) \sin\left(\frac{2\pi}{M}n\right) \quad (3.11c)$$

$$\phi_3 = \|a\|^2 \operatorname{Re}(S_A) = \sum_n (x_n x_{n+1} + y_n y_{n+1}) \quad (3.11d)$$

$$\phi_4 = \|a\|^2 \operatorname{Im}(S_A) = \sum_n (x_n y_{n+1} - y_n x_{n+1}). \quad (3.11e)$$

That is, as indicated in equations (3.4) and (3.6), a sequence's centroids and spreads in both domains follow simply from the five entities in equations (3.11). Each of these entities is a function of $2M$ real variables, namely the x and y . If any one entity is extremized while the others are held constant, a linear combination of their gradients must vanish. This condition can be written as

$$\begin{aligned} (0, 0) &\equiv \sum_k L_k \left(\frac{\partial \phi_k}{\partial x_m}, \frac{\partial \phi_k}{\partial y_m} \right) \\ &= 2 \left[L_0(x_m, y_m) + L_1 \cos\left(\frac{2\pi}{M}m\right) (x_m, y_m) + L_2 \sin\left(\frac{2\pi}{M}m\right) (x_m, y_m) \right. \\ &\quad \left. + L_3(x_{m+1} + x_{m-1}, y_{m+1} + y_{m-1}) + L_4(y_{m+1} - y_{m-1}, x_{m-1} - x_{m+1}) \right] \end{aligned} \quad (3.12)$$

which is an identity over m .

All quantities in equation (3.12) are real. If the first component of this identity is added to i times the second, it follows that any MUS must satisfy

$$\begin{aligned} 0 &= \left[L_0 + L_1 \cos\left(\frac{2\pi}{M}m\right) + L_2 \sin\left(\frac{2\pi}{M}m\right) \right] a_m + L_3(a_{m+1} + a_{m-1}) - iL_4(a_{m+1} - a_{m-1}) \\ &= \left\{ L_0 + \sqrt{L_1^2 + L_2^2} \cos\left[\frac{2\pi}{M}(m-s)\right] \right\} a_m \\ &\quad + \sqrt{L_3^2 + L_4^2} \left[e^{i\frac{2\pi}{M}t} a_{m-1} + e^{-i\frac{2\pi}{M}t} a_{m+1} \right] \end{aligned} \quad (3.13)$$

where s and t are related simply to the original Lagrange multipliers. (Again, a superfluous Lagrange multiplier has been included as a formal convenience.) As in section 2.2, the next step is to find values of the Lagrange multipliers for which equation (3.13) has solutions of the desired form. In order to draw a close parallel with equations (2.11) and (2.12), it is convenient to rewrite equation (3.13) as an eigenvalue relation involving an operator of the form

$$\begin{aligned} \hat{\Gamma}(w, s, t, M)a_m &:= 2w^{-2} \left\{ 1 - \cos\left[\frac{2\pi}{M}(m-s)\right] \right\} a_m \\ &\quad - w^2 \left[e^{i\frac{2\pi}{M}t} a_{m-1} - 2a_m + e^{-i\frac{2\pi}{M}t} a_{m+1} \right]. \end{aligned} \quad (3.14)$$

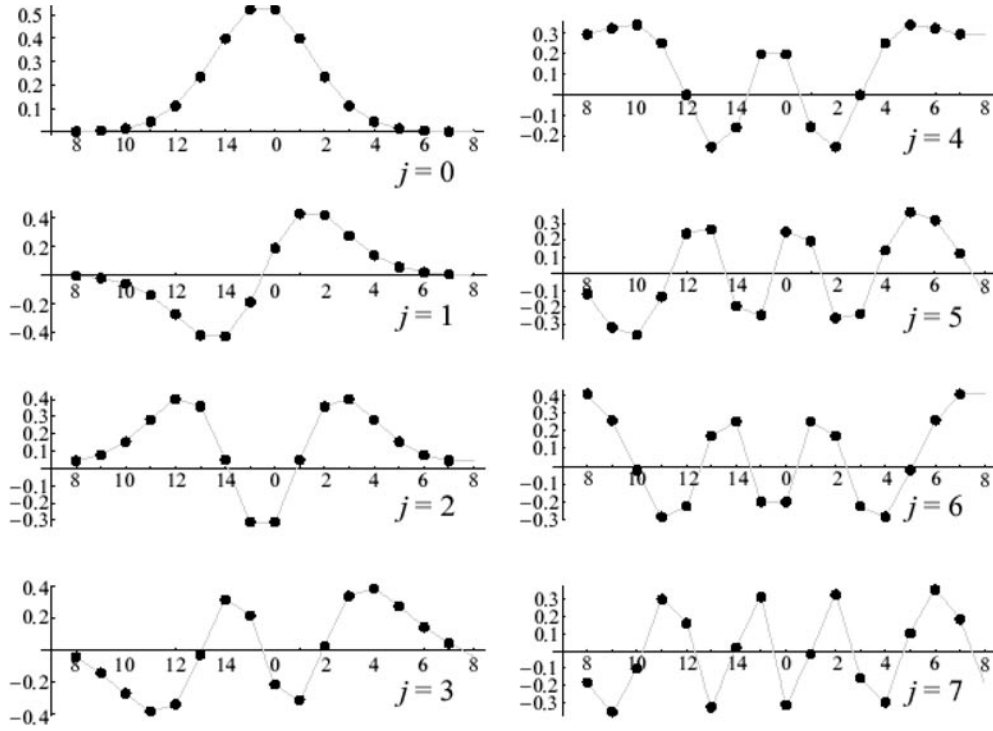


Figure 4. Plots of the first eight eigenvectors for the case $M = 16$ (with half-integral s and $t = 0$). These eigenvectors always display a clear resemblance to the familiar Hermite–Gaussian functions. Note the states have been translated so that the zeroth element sits at the centre of each plot.

This operator can be represented by a tridiagonal Hermitian matrix that multiplies the vector with elements a_m . The identification of equation (3.13) as $\hat{\Gamma}a_m = \lambda a_m$ is straightforward once equation (3.13) is multiplied throughout by a factor of $[(L_1^2 + L_2^2)(L_3^2 + L_4^2)/4]^{-1/4}$.

The discrete analogues of the Hermite–Gaussian functions are proportional to the normalized eigenvectors of $\hat{\Gamma}$. That is, they are given by sequences of numbers $\phi_m^{(j)}$ defined by the relation

$$\hat{\Gamma}\phi_m^{(j)}(w, s, t, M) = \lambda_j(w, s, t, M)\phi_m^{(j)}(w, s, t, M) \quad (3.15)$$

for $j = 0, 1, 2, \dots, M - 1$. It follows from equation (3.14) that $\hat{\Gamma}$ is Hermitian, hence its eigenvalues are real. Note that, as written in equation (3.14), $\hat{\Gamma}$ is a sum of two terms, one of which is diagonal and clearly positive semi-definite. As follows from equations (3.2) and (3.3), the other takes the form of the former’s DFT conjugate, so it is also positive semi-definite. The eigenvalues of $\hat{\Gamma}$ are therefore non-negative (and it is not difficult to show that they are strictly positive). We choose to order them in increasing magnitude, i.e. λ_0 is the smallest. Also, the eigenvectors form a complete set and, for distinct eigenvalues, they are orthogonal,

$$\sum_m \phi_m^{(j)*}(w, s, t, M)\phi_m^{(j')}(w, s, t, M) = \delta_{j,j'} \quad (3.16)$$

when $\lambda_j(w, s, t, M) \neq \lambda_{j'}(w, s, t, M)$. (For degenerate eigenvalues, the eigenvectors can be orthogonalized as a separate step.) A sample of eigenvectors is plotted in figure 4.

In contrast to the results in section 2, however, both the eigenvalues and the eigenvectors now depend on w, s and t , as well as on M . It is evident from the definition of $\hat{\Gamma}$ that integer

changes in s and t do not change the eigenvalues, but generate an index shift and a linear phase factor, respectively, on the eigenvectors,

$$\lambda_j(w, s+k, t+\ell, M) = \lambda_j(w, s, t, M) \quad (3.17a)$$

$$\phi_m^{(j)}(w, s+k, t+\ell, M) = e^{i2\pi\ell m/M} \phi_{m-k}^{(j)}(w, s, t, M) \quad (3.17b)$$

where k and ℓ are integers. Note that, although the eigenvectors are taken to be normalized, each has an arbitrary global phase factor. (Thus, in general, there is the possibility of an extra phase term in equation (3.17b).) The effect of continuous variation in the parameters of the ground state is illustrated in figure 5. Changing the width and centroids evidently has precisely the expected effect.

3.3. Lower limit for the conjugate width

Any sequence can now be expressed in terms of $\hat{\Gamma}$ eigenvectors,

$$a_m = \sum_{j=0}^{M-1} c_j(w, s, t, M) \phi_m^{(j)}(w, s, t, M) \quad (3.18)$$

where

$$c_j(w, s, t, M) = \sum_m \phi_m^{(j)*}(w, s, t, M) a_m. \quad (3.19)$$

In the usual way, the norm defined in equation (3.5) can be shown to satisfy

$$\|a\|^2 = \sum_{j=0}^{M-1} |c_j(w, s, t, M)|^2 \quad (3.20)$$

and it follows similarly that

$$\sum_m a_m^* \hat{\Gamma} a_m = \sum_{j=0}^{M-1} \lambda_j(w, s, t, M) |c_j(w, s, t, M)|^2. \quad (3.21)$$

However, it follows from equation (3.14) that

$$\begin{aligned} \sum_m a_m^* \hat{\Gamma} a_m &= 2\|a\|^2 \left(w^{-2} \left\{ 1 - |S_a| \cos \left[\frac{2\pi}{M}(s - \mu_a) \right] \right\} \right. \\ &\quad \left. + w^2 \left\{ 1 - |S_A| \cos \left[\frac{2\pi}{M}(t - \mu_A) \right] \right\} \right). \end{aligned} \quad (3.22)$$

Upon combining equations (3.20), (3.21) and (3.22), an analogue of equation (2.21) results:

$$\begin{aligned} &w^{-2} \left\{ 1 - |S_a| \cos \left[\frac{2\pi}{M}(s - \mu_a) \right] \right\} + w^2 \left\{ 1 - |S_A| \cos \left[\frac{2\pi}{M}(t - \mu_A) \right] \right\} \\ &= \sum_{j=0}^{M-1} \lambda_j(w, s, t, M) |c_j(w, s, t, M)|^2 \bigg/ 2 \sum_{j=0}^{M-1} |c_j(w, s, t, M)|^2 \\ &\geq \frac{1}{2} \lambda_0(w, s, t, M). \end{aligned} \quad (3.23)$$

Upon isolating $|S_A|$ in equation (3.23), it is possible to consider choosing s , t and w in order to minimize the resulting upper bound. Since the dependence of λ_0 on its arguments is non-trivial, however, this approach cannot be completed in closed form.

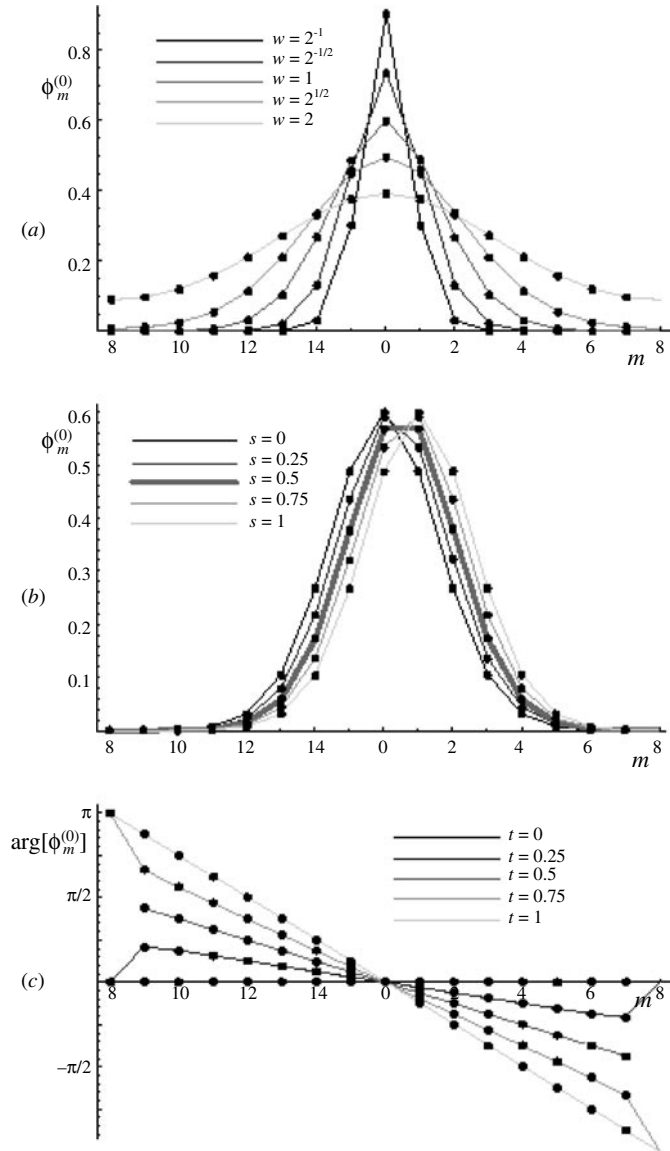


Figure 5. (a) The zeroth eigenstate is plotted for various values of w with $s = t = 0$. (b) The zeroth eigenstate is plotted for various values of s with $t = 0$. The case $s = 0.5$ is shown with a thick connecting line to highlight this Gaussian analogue that is centred at a mid-point. (c) The phase of the zeroth eigenstate is plotted for various values of t with $s = 0$. Note that, when $t = 0.5$, a_8 vanishes, so the phase is indeterminate at that point.

Fortunately, an alternative approach of the type discussed after equation (2.22) remains straightforward: if only the ground state contributes to the sums, the bound can be attained. That is, the task is now to find values of s , t and w for which the ground state, i.e. $\phi_m^{(0)}$, has a centroid, mean frequency and width that match the prescribed values of μ_a , μ_A and σ_a . Of course, this is feasible only when the relation in equation (3.10) is satisfied.

By anticipating that the modulus of the ground state will take the form of a single-lobed Gaussian-like distribution, it is possible to deduce the position at which the curve marking out the perimeter of the accessible domain in (σ_a, σ_A) -space will meet the limit given in equation (3.10). When $\mu_a \neq 0$, at least two coefficients must be non-zero. In particular, in the limit of high localization with $0 < \mu_a < \frac{1}{2}$, all but a_0 and a_1 can be expected to vanish. It follows from equations (3.4)–(3.6) that

$$\tan\left(\frac{2\pi}{M}\mu_a\right) = (1 - \alpha^2) \sin\left(\frac{2\pi}{M}\right) / \left[\alpha^2 + (1 - \alpha^2) \cos\left(\frac{2\pi}{M}\right)\right] \quad (3.24)$$

$$|S_A| = |a_0^* a_1| / \|a\|^2 = \alpha \sqrt{1 - \alpha^2} \quad (3.25)$$

where $\alpha := |a_0| / \|a\|$. Upon solving equation (3.24) for α and using the result in equation (3.25), it follows that the bound associated with the ground state will meet the limit set by equation (3.10) at

$$\sigma_A = \sqrt{1 - \frac{\sin\left(\frac{2\pi}{M}\mu_a\right) \sin\left[\frac{2\pi}{M}(1 - \mu_a)\right]}{\left\{\sin\left(\frac{2\pi}{M}\mu_a\right) + \sin\left[\frac{2\pi}{M}(1 - \mu_a)\right]\right\}^2}}. \quad (3.26)$$

Recall that $\sigma_A := \sqrt{1 - |S_A|^2}$. When σ_A exceeds the value given in equation (3.26), pure eigenstates other than the ground state must set the boundary of the accessible region in (σ_a, σ_A) -space. As with equation (3.10), a partner to equation (3.26) follows upon exchanging a and A throughout.

Symmetry can be used to show that when both s and t are either integers or half-integers, μ_a and μ_A are similarly restricted (i.e. again either integer or half-integer). This observation greatly simplifies the process of finding the values of s and t that give the desired solutions when (μ_a, μ_A) is either $(0, 0)$, $(0, \frac{1}{2})$, $(\frac{1}{2}, 0)$ or $(\frac{1}{2}, \frac{1}{2})$. Because of the symmetry between the DFT and its inverse, the middle two cases are trivially related. We therefore restrict our attention to just three cases, namely $(0, 0)$, $(0, \frac{1}{2})$ and $(\frac{1}{2}, \frac{1}{2})$. It turns out, however, that odd and even values of M require separate treatments. Note that the partner to equation (3.26) (with a and A exchanged) indicates that the section of the boundary of the accessible region that is traced out by the ground state is expected to extend only out to $\sigma_a = \sqrt{3}/2$ for all M when $\mu_A = \frac{1}{2}$. We emphasize that solutions can be found in much the same way for any values of (μ_a, μ_A) ; the special cases considered here are sufficient to illustrate the results.

3.4. Bounds for even values of M

The accessible region of (σ_a, σ_A) -space for $M = 4$ is shown in figure 6(a) for the three selected values of (μ_a, μ_A) . The region excluded by the bounding curve for the case $(\mu_a, \mu_A) = (0, 0)$ is shaded in black. The points on the curve are found by computing the ground state for various values of w with $s = t = 0$ in all cases. The simple algebraic bound given in equation (3.8) is shown as the dashed white line. The MUSs evidently mark out a significantly strengthened inequality. It so happens that the strengthened bound for $M = 4$ coincides precisely with the bound for $M = 2$ (which was discussed in the paragraph preceding equation (3.9)).

The boundary curve for $(\mu_a, \mu_A) = (0, \frac{1}{2})$ is shown as the dashed grey line. Even more of the space is excluded in this case, i.e. the uncertainty relation is now even stronger. This curve is made up of two components. The first segment has negative slope and is found by determining the ground state for various values of w , while the remaining segment

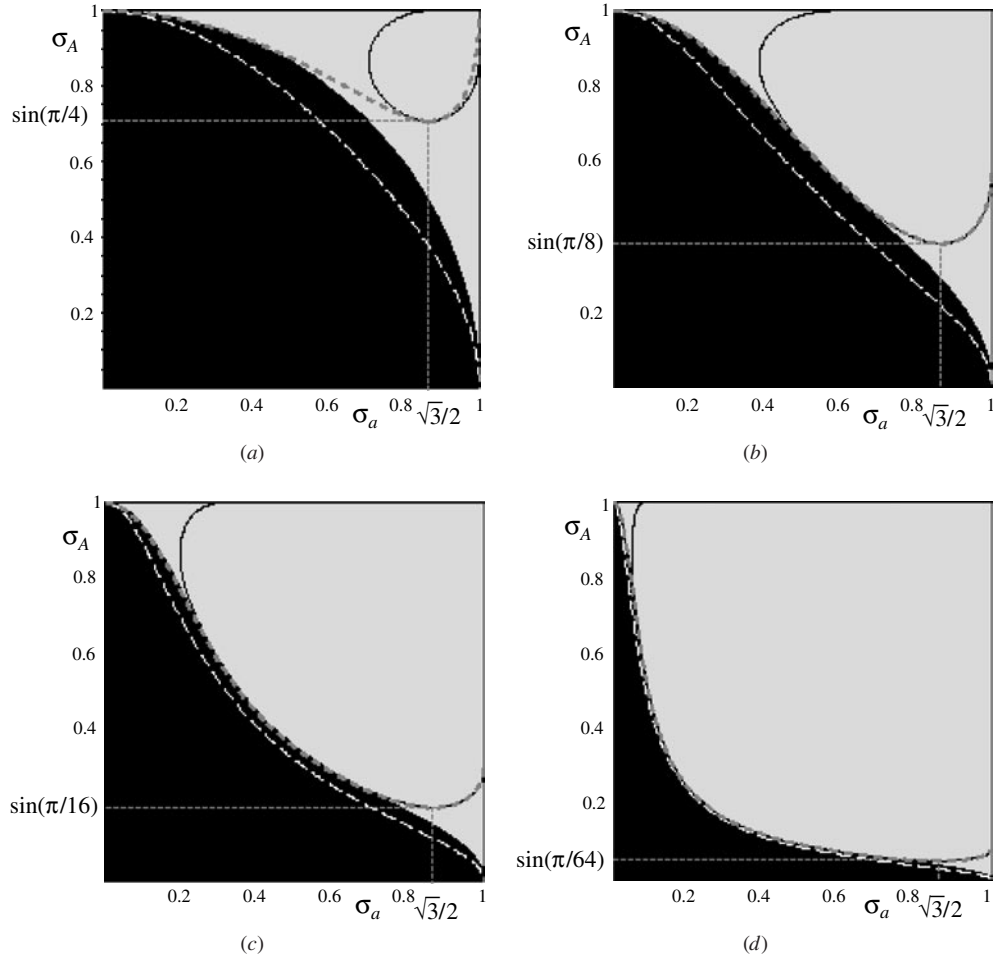


Figure 6. The spreads for any sequence and its DFT conjugate must map to a point that sits in a region that is bounded by a curve within the unit square having coordinates (σ_a, σ_A) . The curve is found to depend on μ_a and μ_A . The curves are shown for (a) $M = 4$, (b) $M = 8$, (c) $M = 16$ and (d) $M = 64$. The white dashed curves are given by the weak bound presented in equation (3.8). It turns out that only the light-grey region is accessible when $(\mu_a, \mu_A) = (0, 0)$. The dashed grey line shows that the boundary is even higher for $(\mu_a, \mu_A) = (0, \frac{1}{2})$. The tightening is even more extreme for $(\mu_a, \mu_A) = (\frac{1}{2}, \frac{1}{2})$, as shown by the solid black line.

(for $\sigma_a > \sqrt{3}/2$) uses the first excited state. In both cases, $s = 0$ and $t = \frac{1}{2}$ while w is varied in order to sweep out the curves. When this curve reaches $(\sigma_a, \sigma_A) = (1, 1)$, it turns out that the first excited state is degenerate. Such degeneracies often introduce subtleties in these calculations. Also note that the curve for the case $(\mu_a, \mu_A) = (\frac{1}{2}, 0)$ can be found by interchanging the axes (i.e. reflecting the plot about the 45° line).

The black curve in figure 6(a) corresponds to $(\mu_a, \mu_A) = (\frac{1}{2}, \frac{1}{2})$. The area of the admissible region is clearly smallest for this case. This curve is made up of three segments, although it involves only two of the eigenstates. The segment where the curve has negative slope is found by computing the ground state for various values of w , while the other two

segments use the first excited state. In all cases, $s = t = \frac{1}{2}$, and w is varied in order to sweep out the curves. Note that this composite curve no longer corresponds to a single-valued function. In the region where it is double valued (i.e. σ_a just larger than $\sin(\pi/4)$), there is evidently not only a minimum uncertainty state for each value of σ_a , but there is sometimes a non-trivial *maximum uncertainty state*. That is, the largest possible value of σ_A is sometimes less than unity.

The plots described above are also presented for $M = 8, 16$ and 64 in figures 6(b), (c) and (d), respectively. Note that, as M increases, more of the space becomes accessible and all of the bounds approach the simple algebraic relation given in equation (3.8). As discussed in [1], in the limit of large M , this relation corresponds to the standard relation of equation (2.22). For smaller values of M , however, significant differences are associated with the various choices for centroid locations. What is more, the algebraic relation can obviously be strengthened significantly for small M .

3.5. Bounds for odd values of M

When M is odd, the sequences have different symmetry properties. For example, consider a sequence that has an integral value of μ_a , but is highly delocalized (i.e. its centre of mass is close to the centre of the disc). Any change to the sequence that moves the centroid over the centre of the disc will change μ_a to a half-integer when M is odd, but not when M is even. As a result, choosing s or t to be zero can (for some values of w) lead to half-integral values of the eigenstate's centroids when M is odd. This means that extra care is needed in exploring the bounds for these cases.

The accessible regions of the uncertainty domain are plotted in figure 7 for a sample of odd values of M . The graphical conventions are the same as those used in figure 6. Once M reaches 64 or more, there is little apparent difference between the plots for M and for $M + 1$, so we have chosen to present only up to $M = 15$ in figure 7. The boundary for $(\mu_a, \mu_A) = (0, 0)$ in all cases is found by computing the ground state for various values of w with $s = t = 0$. As found by Opatrný [4], this strengthened bound for $\mu_a = \mu_A = 0$ and $M = 3$ turns out to be even more stringent than the bound for $M = 2$. However, this bound progressively loosens for all M beyond 3.

For $M > 3$, the curves for $(\mu_a, \mu_A) = (0, \frac{1}{2})$ are made up of two components. The first segment has negative slope and is found by determining the ground state for various values of w , while the remaining segment (for $\sigma_a > \sqrt{3}/2$) uses the first excited state. In both cases, $s = 0$ and $t = \frac{1}{2}$ while w is varied in order to sweep out the curves. Once again, $M = 3$ is exceptional: the second segment for this case is found by using $s = t = 0$.

For $M > 3$, the curves for $(\mu_a, \mu_A) = (\frac{1}{2}, \frac{1}{2})$ are composed of three segments. The segment where the curve has negative slope is found by computing the ground state for $s = t = \frac{1}{2}$ and various values of w . The other two segments use the first excited state with $s = 0$ and $t = \frac{1}{2}$ for one case, and $s = \frac{1}{2}$ with $t = 0$ for the other. In this case, $M = 3$ is a striking exception because the bound for this case cannot be found by using either integer or half-integer values of s . It turns out that the boundary curve is swept out by using the first excited state with $t = \frac{1}{2}$ and varying w while choosing

$$s = \frac{3}{2\pi} \arg \left[27 - 4w^8 + i \left(9\sqrt{3} + 4w^4 \sqrt{9 - w^8} \right) \right]. \quad (3.27)$$

Thankfully, this is the only instance where these four special cases of integral and half-integral centroids require non-trivial values for the Lagrange multipliers.

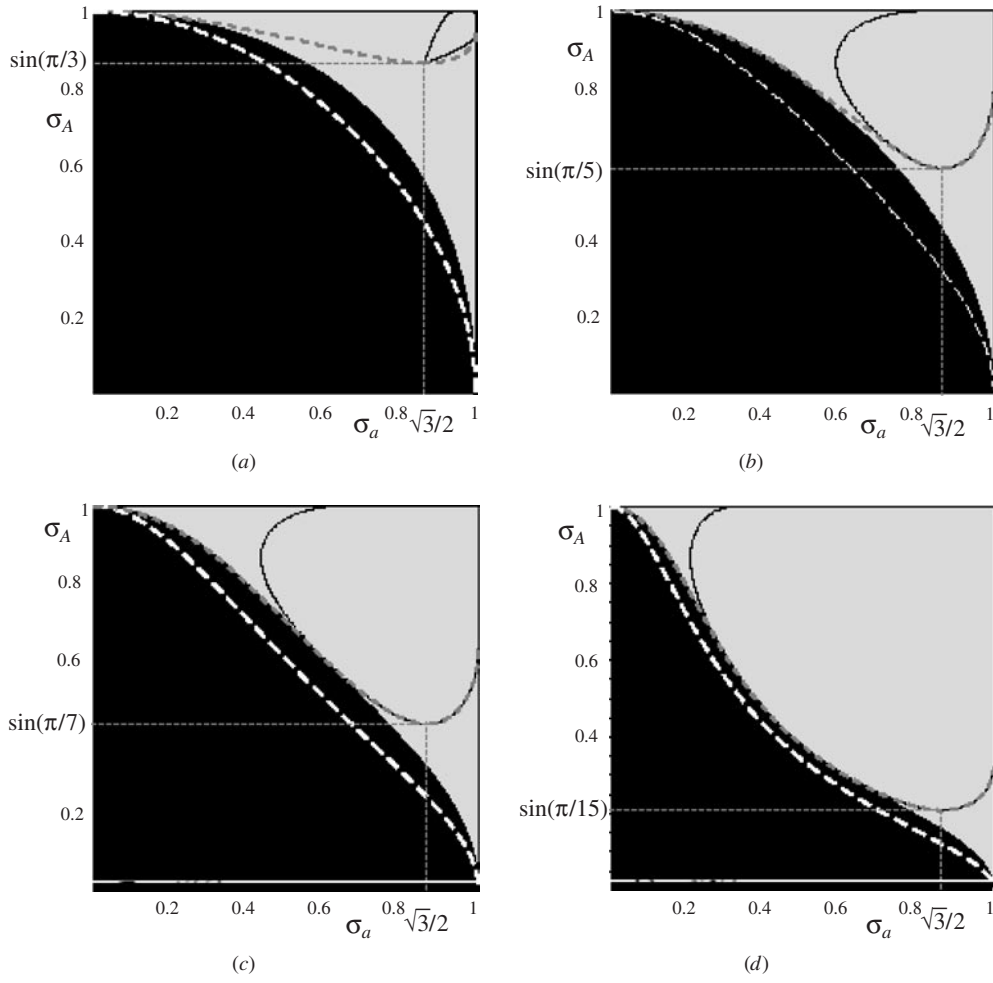


Figure 7. The curves presented in figure 6 are shown here for a sample of odd values of M , namely (a) $M = 3$, (b) $M = 5$, (c) $M = 7$ and (d) $M = 15$.

4. MUSs for the Fourier series

The Fourier series for a continuous function of period 2π takes the form

$$g(\theta) = \frac{1}{\sqrt{2\pi}} \sum_{k=-\infty}^{\infty} G_k e^{ik\theta} \quad (4.1)$$

where

$$G_k := \frac{1}{\sqrt{2\pi}} \int_0^{2\pi} g(\theta) e^{-ik\theta} d\theta. \quad (4.2)$$

Two results that are used repeatedly below follow directly from equations (4.1) and (4.2):

$$\int_0^{2\pi} g^*(\theta)h(\theta) d\theta = \sum_{k=-\infty}^{\infty} G_k^* H_k \quad (4.3a)$$

$$\|g\|^2 := \int_0^{2\pi} |g(\theta)|^2 d\theta = \sum_{k=-\infty}^{\infty} |G_k|^2. \quad (4.3b)$$

The centroid and spread of g are characterized in a similar fashion to that used in the discrete case,

$$\mu_g := \arg(S_g) \quad (4.4a)$$

$$\tau_g := \sqrt{1 - |S_g|^2} / |S_g| \quad (4.4b)$$

where

$$S_g := \frac{1}{\|g\|^2} \int_0^{2\pi} |g(\theta)|^2 e^{i\theta} d\theta = \frac{1}{\|g\|^2} \sum_{k=-\infty}^{\infty} G_k^* G_{k-1}. \quad (4.5)$$

On the other hand, the centroid and spread of the Fourier coefficients are defined in the traditional way as

$$\bar{k} := \frac{1}{\|g\|^2} \sum_{k=-\infty}^{\infty} k |G_k|^2 = \frac{-i}{\|g\|^2} \int_0^{2\pi} g^*(\theta) g'(\theta) d\theta \quad (4.6a)$$

$$\Delta_G^2 := \frac{1}{\|g\|^2} \sum_{k=-\infty}^{\infty} (k - \bar{k})^2 |G_k|^2 = \frac{1}{\|g\|^2} \int_0^{2\pi} g^*(\theta) \left(-i \frac{d}{d\theta} - \bar{k} \right)^2 g(\theta) d\theta. \quad (4.6b)$$

It has been shown [1, 10] that the uncertainty relation for the FS can be written as

$$\tau_g \Delta_G \geq \frac{1}{2}. \quad (4.7)$$

Equality in relation (4.7) can be approached only as either one of the two spreads approaches zero, so this relation can also be strengthened.

The true lower bound is found by following a procedure that is analogous to those adopted in the previous sections. Again, an eigenvalue equation results upon introducing Lagrange multipliers:

$$\hat{\Gamma} g(\theta) := \left\{ 2w^{-2} [1 - \cos(\theta - s)] + w^2 \left(-i \frac{d}{d\theta} - t \right)^2 \right\} g(\theta) = \lambda g(\theta). \quad (4.8)$$

The solutions to equation (4.8) have the form

See endnote 2

$$\begin{aligned} \phi_j(\theta) := & \frac{\exp(it\theta)}{\sqrt{2\pi}} \left(a M_c \left\{ A[-2(j+t), 4w^{-4}], 4w^{-4}, \frac{\theta-s}{2} \right\} \right. \\ & \left. + b M_s \left\{ B[-2(j+t), 4w^{-4}], 4w^{-4}, \frac{\theta-s}{2} \right\} \right) \end{aligned} \quad (4.9)$$

where M_c and M_s are the even and odd Mathieu functions, respectively, and A and B are the so-called Mathieu characteristic values [11, 12]. The coefficients a and b , which depend on j and t , must be chosen to ensure the periodicity of ϕ_j . For example, for the $t = 0$ case, a must be set to zero for odd j while b must vanish for even j . For $t = 1/2$ it is a that must vanish for even j and b for odd j . When t is neither an integer nor a half-integer, both coefficients must be non-zero. (Only when t is neither an integer nor a half-integer are the eigenvalues of both types of Mathieu functions degenerate, so linear combinations are valid solutions to the eigenvalue equation.) Also, as in the discrete case, only when t is either an integer or a half-integer does it coincide with \bar{k} for all w .

In order to show the allowed regions for the uncertainty measures, it is convenient to define finite measures of spread analogous to those in section 3. Thus the spreads of g and G

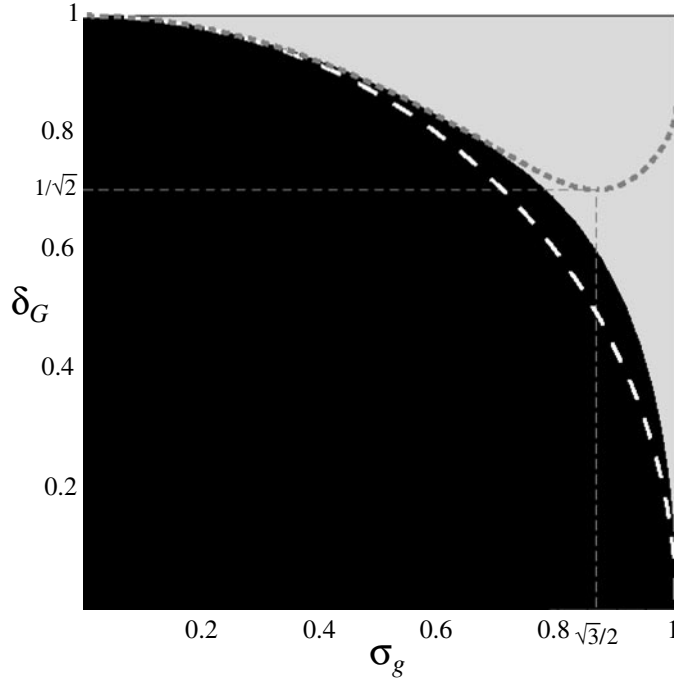


Figure 8. The spreads for a periodic function and its Fourier coefficients must map to a point that sits above a curve within the unit square having coordinates (σ_g, δ_G) . The boundary curve is found to depend on \bar{k} . The white dashed curve is given by the weak bound presented in equation (4.10). It turns out that only the light-grey region is accessible for any integer value of \bar{k} . The dashed dark-grey line corresponds to the boundary (which has moved even higher) when \bar{k} is a half-integer.

are quantified by $\sigma_g := \sqrt{1 - |S_g|^2}$ and $\delta_G := \Delta_G / \sqrt{\Delta_G^2 + 1/4}$, respectively. In these terms, the inequality in equation (4.7) becomes simply

$$\sigma_g^2 + \delta_G^2 \geq 1. \quad (4.10)$$

Figure 8 shows the allowed regions for the uncertainty measures for the two extreme cases, corresponding to \bar{k} being integer and half-integer. These are compared in the figure with the simple algebraic (albeit unattainable) bound of equation (4.10). Note that the bounds are independent of μ_g . The lower bound for integer \bar{k} was obtained from the ground state ($j = 0$, $b = 0$) in equation (4.9), with $t = 0$ and for varying w . As in the DFT case, both the ground state ($j = 0$, $a = 0$) and the first excited state ($j = 1$, $b = 0$) had to be used in generating the lower bound plot for half-integer \bar{k} ($t = \frac{1}{2}$).

5. Concluding remarks

There are a number of surprises that emerged in this analysis. For example, it was unexpected that the uncertainty bounds would be dependent on the positions of a distribution's centroids. Also, given the discussion of equation (2.21), the role of the first excited states in marking out sections of the boundary in sections 3 and 4 is perhaps unintuitive. More strikingly, the notion of non-trivial 'maximum uncertainty states' (as mentioned in section 3.4) enters whenever μ_a ,

μ_A or \bar{k} take non-integer values. Perhaps most unexpected of all, however, was the special treatments that were needed for $M = 3$ in section 3, most notably equation (3.27). Whenever μ_a and μ_A are neither integers nor half-integers, the Lagrange multipliers will be coupled non-trivially (as in equation (3.27)) in order to ensure that the constraints are met, e.g. the centroids sit at the desired positions. This probably cannot be worked through in closed form in all cases: even though we have strived to put the Lagrange multipliers in a consistent and intuitive form (written as w , s and t in sections 2, 3 and 4) their values may need to be found numerically, in general, for the DFT and FS.

The analogues of Hermite–Gaussians that were defined in sections 3 and 4 have a number of interesting properties and potential applications. In the case of the DFT, for example, it can be shown that the eigenstates discussed in section 3 have simple self-Fourier properties much like the conventional Hermite–Gaussians. The complete collection of basis sets (with different values of σ_a , μ_a and μ_A) clearly brings the option for more effective decompositions for a wide range of sequences. As alluded to in the introduction, it also enables some new variants of the fractional DFT to be considered. Of course, Gaussian functions have other interesting properties that help to make them so ubiquitous. For example, their minimum uncertainty character makes them ideal window functions for windowed Fourier transformations in time–frequency analysis. Such optimal windows are now also available for the DFT and the FS. It is the analysis involving Lagrange multipliers and the subsequent reduction to the standard forms given in equations (3.14) and (4.8) (as inspired by equations (2.11) and (2.12)) that enable all of these developments.

Acknowledgments

GWF and MAA are grateful to the Australian Research Council for funds to support this research. MAA also acknowledges funding by the Dirección General de Asuntos del Personal Académico IN112300 Optica Matemática project of the Universidad Nacional Autónoma de México. AES thanks the Air Force Office of Scientific Research for sustained support during his pre-retirement career.

References

- [1] Forbes G W and Alonso M A 2001 *Am. J. Phys.* **69** 1091–95
- [2] Pegg D T and Barnett S M 1997 *J. Mod. Opt.* **44** 225–64
- [3] de Bruijn N G 1967 *Inequalities* ed O Shisha (New York: Academic) pp 57–71
- [4] Opatrný T 1995 *J. Phys. A: Math. Gen.* **28** 6961–75
- [5] Candan C, Kutay M A and Ozaktas H 2000 *IEEE Trans. Signal Proc.* **48** 1329–37
- [6] Barker L, Candan C, Hakioglu T, Kutay M A and Ozaktas H 2000 *J. Phys. A: Math. Gen.* **33** 2209–22
- [7] Ozaktas H, Zalevsky Z and Kutay M A 2001 *The Fractional Fourier Transform with Applications in Optics and Signal Processing* (Chichester: Wiley) pp 201–21
- [8] Forbes G W and Alonso M A 2001 *Am. J. Phys.* **69** 340–7
- [9] Bandilla A and Paul H 1969 *Ann. Phys., Lpz.* **23** 323–33
- [10] Opatrný T 1994 *J. Phys. A: Math. Gen.* **27** 7201–8
- [11] Wolfram S 1999 *The Mathematica Book* 4th edn (New York: Cambridge University Press) p 781
- [12] McLachlan N W 1964 *Theory and Applications of Mathieu Functions* (New York: Dover) p 10

Endnotes

- (1) Author: Please provide PACS number(s).
- (2) Author: Please check the symbols used for Mathieu functions and Mathieu characteristic values in equation (4.9) and the text following it.